Journal of Membrane Science 721 (2025) 123838

Contents lists available at ScienceDirect

Journal of Membrane Science

journal homepage: www.elsevier.com/locate/memsci

Enhanced CO_2 separation performance of mixed-matrix membranes through PIM-1 based surface engineering using non-solvent induced surface deposition

Chanhyuk Kang [a,b,1], Yeji Moon [a,c,1], Joo Eon Kim [c,d], Hyojin Kim [a], Jinhan Cho [b], Jinkee Hong [c], Jaesung Park [d,**], Byoung Gak Kim [a,e,*]

[a] Hydrogen Energy Research Center, Korea Research Institute of Chemical Technology (KRICT), Daejeon, 34114, Republic of Korea
[b] Department of Chemical and Biological Engineering, Korea University, Seoul, 02841, Republic of Korea
[c] Department of Chemical and Biomolecular Engineering, College of Engineering, Yonsei University, Seoul, 03722, Republic of Korea
[d] Green Carbon Research Center, Korea Research Institute of Chemical Technology (KRICT), Daejeon, 34114, Republic of Korea
[e] Department of Chemical Convergence, Materials and Process, University of Science and Technology, Daejeon, 34114, Republic of Korea

ARTICLE INFO

Keywords:
Zeolitic imidazolate framework (ZIF)
Metal-organic framework (MOF)
Polymers of intrinsic microporosity (PIMs)
Mixed-matrix membranes (MMMs)
Gas separation
Carbon dioxide

ABSTRACT

Carbon dioxide (CO_2), a major greenhouse gas, significantly contributes to global warming and negatively affects ecosystems. This necessitates the development of high-performance materials for CO_2 removal. Mixed-matrix membranes (MMMs) incorporating metal-organic frameworks (MOFs) are effective for CO_2 separation, but the poor interfacial compatibility between the polymer and filler often reduces membrane performance. In this study, the interfacial issue in MMMs was addressed by surface modification of ZIF-8 with polymers of intrinsic microporosity (PIM-1) using the non-solvent induced surface deposition method. The PIM-1 polymer on the ZIF-8 surface has a high surface area, which prevents pore blockage and overcomes the interfacial issue with the polymer matrix. The effect was studied using Pebax-1657 as a host polymer matrix. At 20 % loading, MMMs with surface-modified ZIF-8@PIM-1 exhibited enhanced CO_2/N_2 and CO_2/CH_4 selectivities, increasing from 44.4 to 15.1 to 45.6 and 18.8, respectively, compared to those of MMMs with unmodified ZIF-8. In addition, the CO_2 permeability increased by about 40 %, from 71 barrer to 105 barrer, compared to that of pure Pebax-1657. This study demonstrates that simple surface modification with PIM-1 can effectively address the interfacial issues between the polymer matrix and MOF in MMMs.

1. Introduction

Membrane separation technology can effectively remove carbon dioxide (CO_2), a representative greenhouse gas that causes global warming [1,2]. Polymeric membranes are attracting attention as excellent materials for CO_2 removal owing to their low cost, excellent processability, and chemical stability [3–5]. Recent efforts have been made to remove CO_2 using various materials such as polyimide (PI) [6,7], polyphenylene oxide (PPO) [8,9], cellulose acetate (CA) [10,11], and polydimethylsiloxane (PDMS) [12]. Polymeric membranes have low permeability in the range of tens of barrer (10^{-10} cm^3 (STP) cm cm^{-2} s^{-1} cm Hg^{-1}), which limits their ability to effectively separate large amounts of CO_2. To overcome these limitations, various porous materials with high intrinsic permeability have been developed to fabricate high-permeability membranes, but they have not been able to escape the trade-off relationship in polymeric membranes [13–15].

A simple approach to overcome these membrane limitations is to use a novel mixed-matrix membranes (MMMs). MMMs are composite membranes fabricated by introducing inorganic filler materials into a continuous polymer matrix, which significantly improves separation performance by overcoming the trade-off relationships of conventional membranes [16–18]. For instance, metal-organic framework (MOF)--based MMMs efficiently improve gas separation performance by selecting an appropriate MOF for the desired gas pair as a filler [19,20].

* Corresponding author. Hydrogen Energy Research Center, Korea Research Institute of Chemical Technology (KRICT), Daejeon, 34114, Republic of Korea.
** Corresponding author.
E-mail addresses: j.park@krict.re.kr (J. Park), bgkim@krict.re.kr (B.G. Kim).
[1] These authors contributed equally to this work.

https://doi.org/10.1016/j.memsci.2025.123838
Received 5 December 2024; Received in revised form 25 January 2025; Accepted 10 February 2025
Available online 11 February 2025

ZIF-8, a type of MOF, has a pore aperture of 3.4 Å, making it very effective in separating CO_2 from other gases of different sizes; therefore, ZIF-8 is often used as a filler in MMMs [21,22]. However, introducing MOFs such as ZIF-8 into polymer membranes can lead to low affinity and the formation of non-selective voids at the interface, which may limit the performance improvement [23]. This can be addressed by improving the affinity between MOFs and polymer membranes [24,25].

Among the many attempts to solve the interfacial problems of MOF-based MMMs, MOF functionalization is an effective method to improve the affinity between the MOF and polymer by imparting specific functional groups to the surface or internal structure [26]. Many studies have been conducted to control the surface properties and provide chemical and physical stability by introducing various functional groups. MOF functionalization is performed by introducing functional ligands [27,28], ionic liquid modification [29,30], MOF [31], or polymer coating [32–34]. MOF functionalization through polymer coating leads to good affinity with the polymer matrix according to the "like dissolves like" rule and has the potential to impart a wide range of functions depending on the polymer selection. For instance, Jin et al. introduced polydopamine (PD) on the ZIF-8 surface to improve its adhesion properties, thereby solving the interfacial problems between fillers and polymers and showing excellent H_2/N_2 and H_2/CH_4 separation performance [32]. Qiao et al. prepared well-sealed nanoparticles by coating PEG on the MOF surface, which showed excellent CO_2 permeability and CO_2/N_2 selectivity [33]. Moreover, Cohen et al. fabricated defect-free MMMs by removing the boundaries between MOF and polymer using PDMS, and showed high CO_2 permeability and CO_2/N_2 selectivity [34]. To coat the polymer on the MOF surface, a separate polymerization or cross-linking reaction process is required. However, the reaction is difficult to control, limiting mass production and introduction of various polymers. Nevertheless, when polymers are coated on the surface of MOFs, pore blocking may occur, which can reduce permeability. This issue arises because polymers like PD, PEG, and PDMS can block the MOF pores, leading to reduced permeability. Therefore, methods that can easily and efficiently coat various polymers while overcoming pore blocking are required.

Li et al. reported a novel method called non-solvent induced surface deposition (NISD) [35], which can rapidly and easily fabricate MOF@-polymer particles within seconds and enables the introduction of various MOFs and polymers through solvent selection. They used the NISD method to coat the surface of MOF-801 with polyimide, polymer of intrinsic microporosity (PIM-1), or polysulfone, fabricating particles with excellent stability and weatherability and demonstrating their potential in gas storage applications. However, to date, studies exploring the application of this method to mixed-matrix membranes (MMMs) to address the interfacial challenges between the polymer matrix and MOFs remain limited.

PIMs stand out among polymer candidates for coating MOF surfaces. For instance, PIM-1 contains a polybenzodioxane structure with a contorted site in its chemical structure, which prevents efficient packing between polymer chains and has intrinsic microporosity [36]. In addition, PIM-1 is easily processible as it can be dissolved in organic solvents such as chloroform or dichloromethane. PIM-1 is an attractive material for gas separation due to its high Brunauer-Emmett-Teller (BET) surface area of 600–800 m^2/g and high permeability behavior. Polymers other than PIMs often cause pore clogging in MOFs owing to their low BET surface area, thus hindering gas permeation. Coating the MOF surface with PIM-1 can improve the interfacial affinity without hindering the permeation behavior of the MOF owing to its high surface area.

In this study, we report the improved CO_2 separation performance of MMMs incorporating ZIF-8@PIM-1 particles into a Pebax-1657-based polymer matrix using NISD. The PIM-1 coating on the ZIF-8 surface is expected to prevent pore clogging of the filler and solve the compatibility problem between the filler and polymer matrix. The large surface area of PIM-1 prevents pore blockage on the ZIF-8 surface, facilitating gas transport. Additionally, PIM-1 is expected to mitigate the interfacial issues between ZIF-8 and the polymer matrix, allowing for higher filler loading.

2. Experimental section

2.1. Materials

Commercial Pebax® MH 1657 (Arkema Inc.) was used as purchased. Dimethylformamide (DMF, 99.8 %, Sigma-Aldrich), tetrahydrofuran (THF, 99.0 %, Sigma-Aldrich), chloroform (≥99 %, Sigma-Aldrich), potassium carbonate (≥99 %, Sigma-Aldrich), methanol (99.8 %, Sigma-Aldrich), ethanol (99.8 %, Sigma-Aldrich) 5,5′,6,6′-tetrahydroxy-3,3,3′,3′-tetramethyl-1,1′-spirobisindane (TTSBI, SAMCHEN Chemicals), 2-methylimidazole (2-Melm, 99 %, Sigma-Aldrich), zinc nitrate hexahydrate ($Zn(NO_3)_2{\cdot}6H_2O$, 98 %, thermo scientific), and petroleum ether (EA grade, DUKSAN reagents) were used as purchased. Tetrafluoroterephthalonitrile (TFTPN, >98 %, Matrix Scientific) was purified by sublimation at 150 °C under low pressure.

2.2. Synthesis of PIM-1

PIM-1 was synthesized as described in our previous study [37]. All glassware was dried in an oven prior to use. Under a nitrogen atmosphere, a mixture of TTSBI (10.2123 g, 30 mmol), TFTPN (6.0027 g, 30 mmol), and anhydrous K_2CO_3 (8.2923 g, 60 mmol) was dissolved in DMF (210 mL) in a 500 mL 3-necked round bottom flask, which was placed in a preheated heating mantle at 55 °C and maintained for 3 d. The mixture was then cooled, and THF was added to the flask to remove the low-molecular-weight fraction. The yellow polymer was dissolved in THF and reprecipitated from H_2O. After two additional reprecipitation steps, the precipitate was further reprecipitated in methanol. The mixture was then refluxed overnight in methanol. The synthesized PIM-1 polymer was dried in an 80 °C vacuum oven for 2 d. Yield: 11.0 g (79.3 %). ^1H NMR (500 MHz, $CDCl_3$, δ): 6.80 (2H, s), 6.41 (2H, s), 2.46–2.04 (4H, dd), 1.45–1.16 (12H, br). The molar masses (determined from M_n) were $M_n = 75{,}400$, $M_w = 139{,}700$, dispersity ($Đ$) = 1.85. Anal. Calcd for $C_{29}H_{20}N_2O_4$ (wt %): C, 75.64; H, 4.38; N, 6.08; O 13.90. Found: C, 74.09; H, 4.24, N, 5.98; O, 14.00 %. The BET surface area was 875 $m^2\ g^{-1}$.

2.3. Synthesis of ZIF-8 particles

ZIF-8 particles were synthesized following the procedure by He et al. [38]. Specifically, 12.98 g of 2-Melm and 5.866 g of $Zn(NO_3)_2{\cdot}6H_2O$ were dissolved in 100 mL of methanol. After stirring for 1 h at room temperature, the crystals were separated by centrifugation and washed with methanol. The product was dried under vacuum at 80 °C overnight.

2.4. Synthesis of ZIF-8@PIM-1 particles

ZIF-8@PIM-1 core-shell particles were synthesized following the procedure by Li et al. [35]. Specifically, 500 mg ZIF-8, 50 mg PIM-1, and dichloromethane (20 mL) were added and stirred for 1 h to create a well-dispersed solution. After stirring, 40 mL of petroleum ether was added to the vigorously stirred solution, and the ZIF-8@PIM-1 particles rapidly precipitated within a few seconds. The product was collected via centrifugation and washed with petroleum ether. The product was dried under vacuum at 80 °C overnight.

2.5. Membrane fabrication

Pure Pebax-1657 was prepared via solution evaporation. First, Pebax-1657 pellets were dissolved in a mixed solution (70 % ethanol and 30 % water) and refluxed at 80 °C for 2 h. The homogeneously mixed solution was poured into a PTFE petri dish and dried in a 50 °C oven for 48 h. Finally, the membrane was dried under vacuum at 50 °C overnight.

MMMs were prepared using the same method as that used for Pebax-1657. ZIF-8 and ZIF-8@PIM-1 particles were added to the polymer solution at the desired content and ultrasonicated for 30 min for complete dispersion. The solution was dried following the same procedure used for Pebax-1657.

2.6. Characterization

The number-average molecular weight (M_n) and dispersity ($Đ$) of the polymer were determined by size exclusion chromatography (SEC) with an HPLC system (Waters Corporation) using three Shodex columns and a refractive index detector. THF served as the eluent at 1 mL/min at 40 °C. A calibration curve was established using polystyrene standards (molecular weight range: 1.31×10^3 to 3.64×10^6 Da, Showa Denko K·K.). Proton nuclear magnetic resonance (^{1}H NMR) spectroscopy was conducted on AVNCE III HD and AVANCE NEO (Bruker Corporation). Transmission electron microscopy (TEM) was performed using high resolution double Cs corrected transmission electron microscopy (HR-TEM, Spectra Ultra). Field-emission scanning electron microscopy (FE-SEM) was conducted using Gemini 560 (Carl Zeiss). Thermogravimetric analysis (TGA) was performed using a Discovery TGA5500 (TA instruments) between 30 and 800 °C under nitrogen flow at a heating rate of 10 °C min^{-1}. X-ray diffraction (XRD) analysis was performed using a D8 ADVANCE (Bruker). Ultraviolet–visible diffuse reflectance spectroscopy (UV–Vis DRS) was performed using a Cary 5000 (Agilent). Fourier transform infrared spectroscopy (FT-IR) measurements were recorded using a ALPHA-T spectrometer (Bruker). Each sample was scanned 128 times at a resolution of 4 cm^{-1} in the range 4000–500 cm^{-1}. Elemental analysis (EA) was obtained on a FLASH EA-2000 Organic Elemental Analyzer (Thermo Scientific). X-ray photoelectron spectroscopy (XPS) was conducted using an AXIS SUPRA (KRATOS) with a monochromatic Al-Kα source (15 KeV). The surface area and pore size distribution were calculated with Micromeritics ASAP 2020 instrument. The sample was dried for 5 h at 100 °C before analysis. Nitrogen sorption isotherms were also obtained from the Micromeritics ASAP 2020 instrument at 77 K and pressure ranging from 0.01 to 1 bar. Dispersion stability was evaluated at 30 min intervals for 24 h using Turbiscan LAB (Formulaction).

2.7. Pure gas permeation experiments

The pure gas permeation properties of the prepared MMMs were measured using a time-lag method called the constant-volume variable-pressure method at 35 °C and at a feed pressure of 3 bar. The downstream pressure was measured by using a manometer (MKS Baratron 627F). Gas permeation (p) was calculated using the following equation:

$$p\left(10^{-6}\frac{\mathrm{cm^3(STP)}}{\mathrm{cm^2 s \bullet cm \bullet Hg}}\right) = \frac{V_d}{p_2 ART}\left[\left(\frac{dp_1}{dt}\right)_{ss} - \left(\frac{dp_1}{dt}\right)_{leak}\right] \quad (1)$$

where V_d is the downstream volume, p_2 is the upstream pressure, A is the area of the membrane, (dp_1/dt) is the leak rate of the time-lag device, and $(dp_1/dt)_{ss}$ is the steady-state pressure change during the measurement.

Gas permeability (P) is calculated by the following equation.

$$P = p \times l \quad (2)$$

where p is the previously calculated gas permeance and l is the polymer membrane thickness.

The ideal selectivity (α) of the two different gases was calculated by the following equation using the permeability calculated by the time-lag method.

$$\alpha_{AB} = P_A / P_B \quad (3)$$

2.8. Gas sorption measurements

The sorption of CH_4 and CO_2 by the materials was determined using a pressure-decay method with a dual-volume dual-transducer sorption system [39,40]. This system consists of two chambers, a sample cell, and a charge cell, both equipped with pressure transducers (Model PMP5074 series, GE, USA). The cell volumes were calibrated using the Burnett expansion method [41]. Before the measurements, the system was evacuated overnight to remove any dissolved gases from both the samples and apparatus. Sorption isotherms were obtained by measuring gas uptake as a function of increasing pressure, ranging from 3 to 14 atm at 35 °C. All data were recorded using a GraphTec data logger (Model GL240, GraphTec, Japan). From the sorption isotherms, the apparent solubility coefficients (S) were calculated as the ratio of the concentration (C) to pressure (p) as follows [42]:

$$S = C/p$$

3. Result and discussion

3.1. Characterization of ZIF-8@PIM-1 particles

Fig. 1a–c shows the chemical structure of each material used to fabricate the MMMs. Pebax-1657 has excellent mechanical strength owing to its rigid polyamide segment and good affinity for polar gas due to the soft polyether segment (Fig. 1a); therefore, it was selected as a candidate group for the polymer membrane. ZIF-8 has a pore aperture of 3.4 Å and is effective in separating CO_2 and other gases (Fig. 1b), so it was used as an inorganic filler. The ZIF-8 surface was coated with PIM-1 (Fig. 1c) to solve the interface problem between the polymer membrane and inorganic filler. PIM-1 is a polymer with its own contorted structure and has the advantages of a high BET specific surface area and solution processability. The PIM-1-based surface deposition layer can solve the interfacial problem by improving the difference in surface properties between the polymer matrix and ZIF-8 that occurs during the evaporation process, and prevent the pore clogging of ZIF-8, thereby preventing the reduction of the permeability of MOF. Moreover, when selecting the filler, deposition polymer, and polymer matrix, it is crucial to avoid the potential for the deposition polymer and polymer matrix to dissolve in the same solvent. To prevent such issues, careful evaluation of the solubility differences is necessary to ensure the appropriate combination is selected.

The ZIF-8@PIM-1 particles were prepared using the NISD method developed by Li et al. [35]. and illustrated in Fig. 1d. The PIM-1 and ZIF-8 were dissolved and dispersed in the good solvent, dichloromethane. Upon adding excess poor solvent, PIM-1 coated the surface of the ZIF-8 particles owing to surface deposition induced by the non-solvent. The mechanism involves three stages. First, the addition of a poor solvent tends to exclude the dissolved polymer, causing nucleation on the MOF surface. Second, a uniform coating was formed through the continuous deposition of the polymer on the ZIF-8 surface. Finally, precipitation occurred because of the aggregation of the ZIF-8@PIM-1 composite particles. This process is completed within a few seconds, enabling rapid preparation. The precipitated particles were separated by centrifugation and vacuum-dried.

Transmission electron microscopy (TEM) and scanning electron microscopy (SEM) analyses were performed to confirm the successful fabrication of ZIF-8@PIM-1. Fig. 2 and Fig. S1 show TEM, SEM, and optical images of the ZIF-8 and ZIF-8@PIM-1 particles, respectively. As shown in Fig. 2a, the well-fabricated ZIF-8 exhibited a polyhedral crystal structure with a diameter of approximately 100–200 nm as previously reported [43,44]. The polymer-coated ZIF-8@PIM-1 particles still exhibited a polyhedral crystal structure, and the polymer coating on the particle surface was confirmed, as shown in Fig. 2b. Fig. S1 shows the dispersion and agglomeration of the particles after polymer coating, confirming that excellent particle dispersion was maintained after the

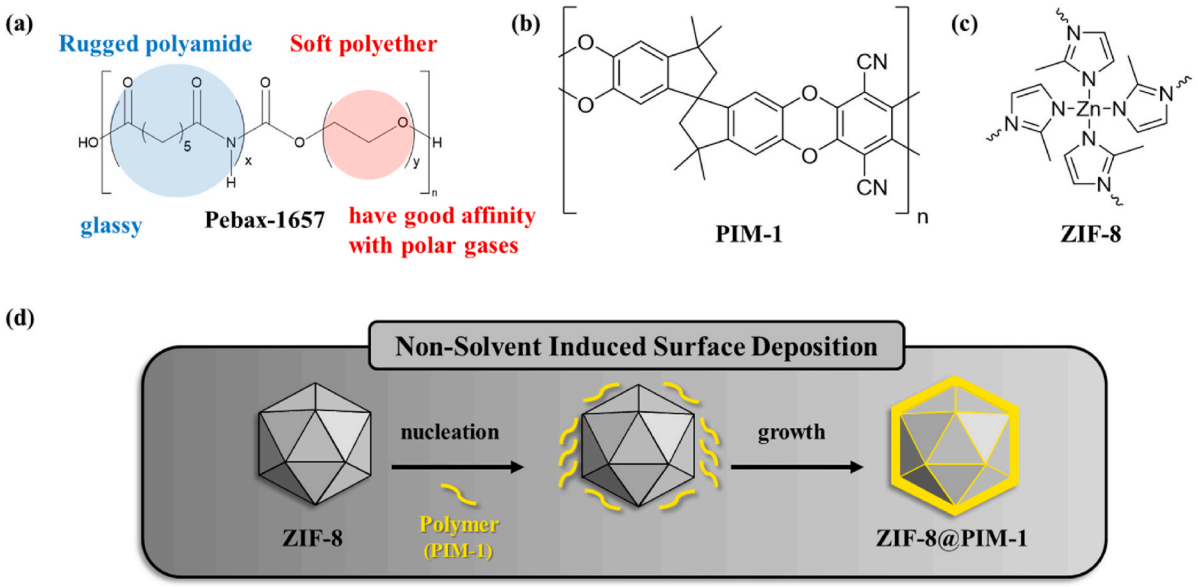

Fig. 1. Chemical structure of (a) Pebax-1657, (b) PIM-1 and (c) ZIF-8; (d) schematic illustration of the non-solvent induced surface deposition (NISD) process.

polymer coating. Fig. 2c and d shows the SEM images of the particles. In contrast to the clear polyhedral crystal structure of ZIF-8, the polymer-coated ZIF-8@PIM-1 particles exhibited rough surfaces with visible polymer clusters. In addition, PIM-1 showed a fluorescent yellow color. ZIF-8 appeared white, but the surface-coated ZIF-8@PIM-1 particles were fluorescent yellow, similar to PIM-1, as confirmed in Fig. 1e and f.

After the fabricated particles were dispersed in water, a dispersion stability test was performed using a turbiscan device to confirm their sedimentation tendency. Fig. 3 shows the sedimentation tendency of each particle over time at a height of 10 mm in a solution with a total height of 40 mm. The ZIF-8 solution showed almost no sedimentation even after 24 h. However, for the ZIF-8@PIM-1 solution, many particles were confirmed to have sedimented after 24 h. This occurs because the hydrophobic PIM-1 covers the surface of ZIF-8, changing its affinity for the polar solvent, water. The decrease in dispersion stability of the ZIF-8@PIM-1 particles was caused by surface modification of PIM-1.

To further confirm the presence of PIM-1 in the fabricated ZIF-8@PIM-1, ultraviolet–visible diffuse reflectance spectroscopy (UV–Vis DRS), fourier transform infrared (FT-IR) spectrosocopy, elemental analysis (EA) and X-ray photoelectron spectroscopy (XPS) were performed. Fig. S2 shows the UV–Vis DRS spectra of the ZIF-8, ZIF-8@PIM-1 particles, and PIM-1 powder. The ZIF-8 particles show peaks at 213, 300, and 412 nm, which are typical of ZIF-8. The PIM-1 powder exhibited peaks at 302 and 412 nm. The ZIF-8@PIM-1 powder exhibits three peaks at 213, 302, and 440 nm, confirming the coexistence of ZIF-8 and PIM-1.

Fourier transform infrared (FT-IR) measurements were performed to investigate the interactions within the ZIF-8@PIM-1. Fig. S3 shows the FT-IR spectra of ZIF-8, ZIF-8@PIM-1, and PIM-1. For ZIF-8, the peak at 1583 cm^{-1} represents the absorption of the C═N stretching vibration of the imidazole ring. The peaks at 1310, 1146, and 993 cm^{-1} are due to the in-plane bending vibration of the imidazole ring. The peaks at 758 and 692 cm^{-1} are due to the out-of-plane bending vibration of the imidazole ring. For PIM-1, the C–O stretching peaks appear at 1265 and 1001 cm^{-1}. In addition, the substituted aromatic ring peak appears at 878 cm^{-1}. In ZIF-8@PIM-1, in addition to the ZIF-8 peaks, the characteristic peaks of PIM-1 appear at 1265, 1001 and 878 cm^{-1}, confirming no additional chemical bonds.

EA was performed to quantitatively confirm the presence of PIM-1 in the ZIF-8@PIM-1 particles, as listed in Table 1. Pure ZIF-8 ideally have no oxygen (O) element, but 2.96 wt% O was observed due to Zn–O generated by the oxidation of ZIF-8 [45,46]. Compared with ZIF-8, PIM-1 has a very high proportion of carbon (C) at 74.1 wt%, and O is clearly present at 14.0 wt%. When examining ZIF-8@PIM-1, the C and O contents have increased compared to pure ZIF-8. This result confirmed the presence of 4.18 % PIM-1 when the increase in C was calculated based on Zn.

XPS was performed to prove that PIM-1 was well coated on the surface of the ZIF-8 particles, as summarized in Fig. S4. Pure ZIF-8 was composed of N, C, and Zn, whereas PIM-1 was composed of C, H, N, and O, among which carbon was the most abundant at 74.1 wt%. Therefore, when the surface was coated with PIM-1, the intensity of the peaks corresponding to pure ZIF-8 decreased, and the intensity of the peaks corresponding to PIM-1 increased. As illustrated in Fig. S4a, the binding energy of N 1s at 399.8 eV and 399.0 eV can be ascribed to N–Zn and N–C. For ZIF-8@PIM-1, the peak corresponding to pure ZIF-8 decreases and a new N ≡ C peak is formed at 399.5 eV (Fig. S4b). Fig. S4c and d show the C 1s spectrum, with peaks at 288.6 eV, 288.5 eV, and 284.5 eV, corresponding to C–O, C–N, and C–C, respectively. As mentioned earlier, the overall peak intensity was high because of the high carbon content of PIM-1. Fig. S4e and f show the O 1s spectra. For ZIF-8 (Fig. S4e), the peaks at 533.0 eV and 532.0 eV represent O–C and O–Zn, respectively. For ZIF-8@PIM-1, Fig. S4f confirms that the intensity of the 533.0 eV peak increased due to the C–O in PIM-1. Fig. S4g and f show the Zn 2p spectra, with peaks at 1045 and 1022 eV corresponding to Zn 2p3/2 and Zn 2p1/2, respectively. After coating with PIM-1, the intensities of the two peaks decreased. Overall, the XPS analysis confirmed the successful PIM-1-based surface modification of ZIF-8.

The BET surface area, pore volume, and pore size of ZIF-8 and ZIF-8@PIM-1 particles are listed in Table 2. The surface areas are 1697 m2/g for ZIF-8, 1659 m2/g for ZIF-8@PIM-1, and 875 m2/g for PIM-1, respectively. The total pore volumes of each particle are 1.39 cm3/g for ZIF-8 and 1.37 cm3/g for ZIF-8@PIM-1. The PIM-1 has a pore volume of 0.662 cm3/g, which is a relatively high pore volume for a general polymer. The pore size of each particle was measured by the Horvath–Kawazoe method, and the pore size distribution is shown in Fig. S5. For ZIF-8, it is 0.699 nm, for ZIF-8@PIM-1, it is 0.694 nm, and for PIM-1, it is 0.981 nm. Although the pore size distribution measured under N_2 gas has limitations in measuring small micropores less than 5 Å, it can play a role in observing the change of pore size. Our results argue that the pore size of ZIF-8 is still maintained after the introduction of PIM-1, which prevents the micropore clogging phenomenon. The

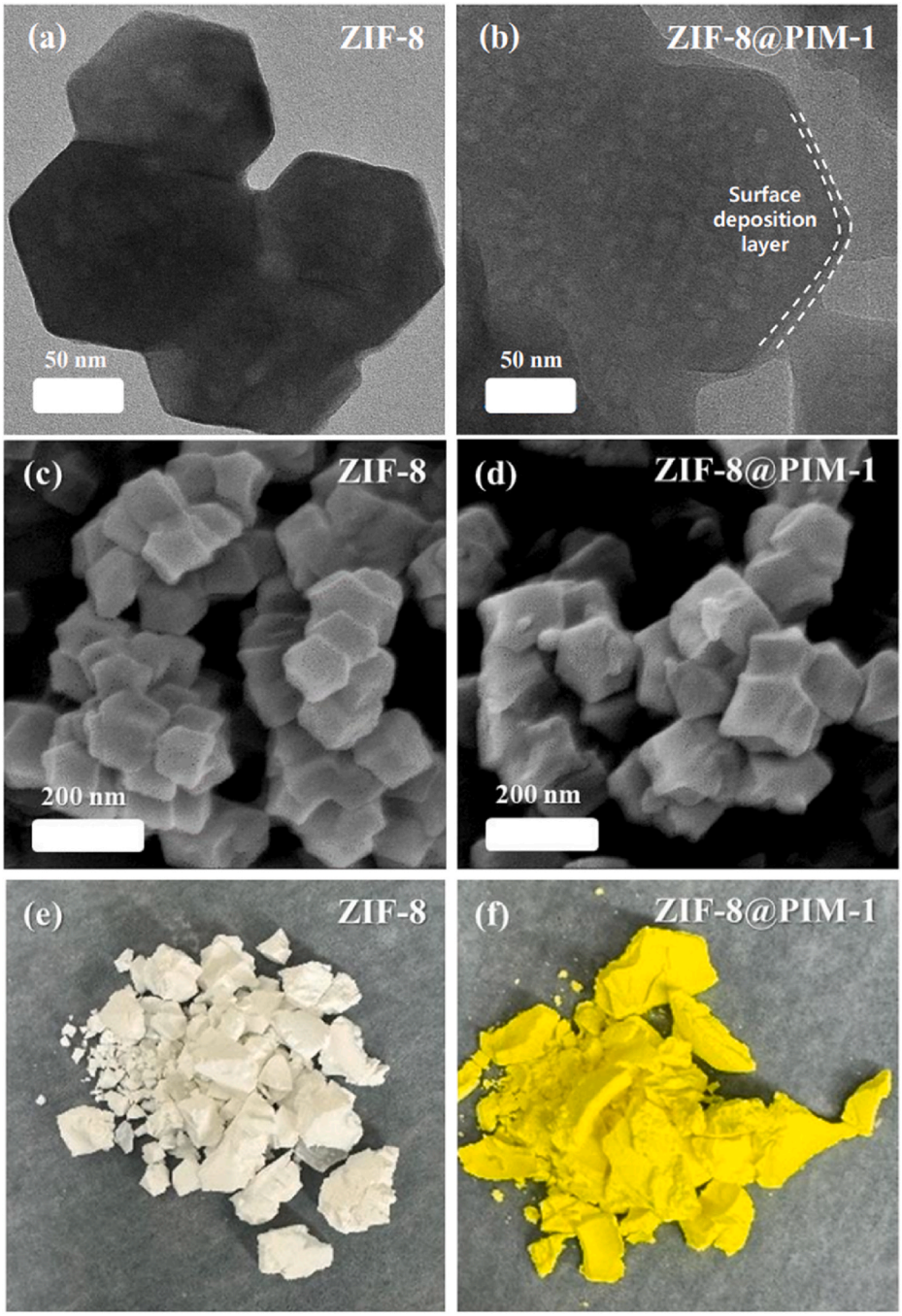

Fig. 2. TEM images of (a) ZIF-8 and (b) ZIF-8@PIM-1 particles; FE-SEM images of (c) ZIF-8 and (d) ZIF-8@PIM-1 particles; photographs of (e) ZIF-8 and (f) ZIF-8@PIM-1 samples.

surface modification of PIM-1 with excellent porosity can prevent the micropore clogging of ZIF-8. This can effectively prevent the unexpected decrease of gas permeability and improve the interfacial compatibility with the polymer matrix.

The specific BET surface area can be obtained from the N_2 isotherm curve in Fig. 4a. The ZIF-8 particles exhibit reversible type-I isotherms. The rapid increase in the amount of nitrogen adsorbed at low pressure ($P/P_0 < 0.08$) indicated that the sample had micropores. In addition, when $P/P_0 = 1$, the rapid increase suggests the mesoporosity and macroporosity of the ZIF-8 particles. Meanwhile, PIM-1 exhibits type IV isotherms, where a very large hysteresis can be seen in the description curve. This is typical of PIM-1 owing to gas molecules adsorbed to the polymer or due to pore swelling. The ZIF-8@PIM-1 particles coated with PIM-1 exhibited a type I shape and the same pattern as that of ZIF-8. This confirmed the well-maintained microporosity of ZIF-8.

The amount of coated PIM-1 on the synthesized ZIF-8@PIM-1 particles was determined by thermogravimetric analysis (TGA). Fig. 4b shows the TGA results for ZIF-8, ZIF-8@PIM-1, and PIM-1. PIM-1, which has a main chain and has high thermal stability up to 480 °C, shows significant weight loss by polymer chain decomposition and ether bond removal. ZIF-8 exhibits two weight-loss steps. The first is a weight loss due to the removal of the guest molecule (mainly H_2O), and the second step is a major mass loss at around 500 °C. Before the decomposition of PIM-1 begins, ZIF-8@PIM-1 shows better thermal stability than ZIF-8, indicating that coating PIM-1 on the surface of ZIF-8 improves its thermal stability. After 650 °C, the mass difference between ZIF-8 and

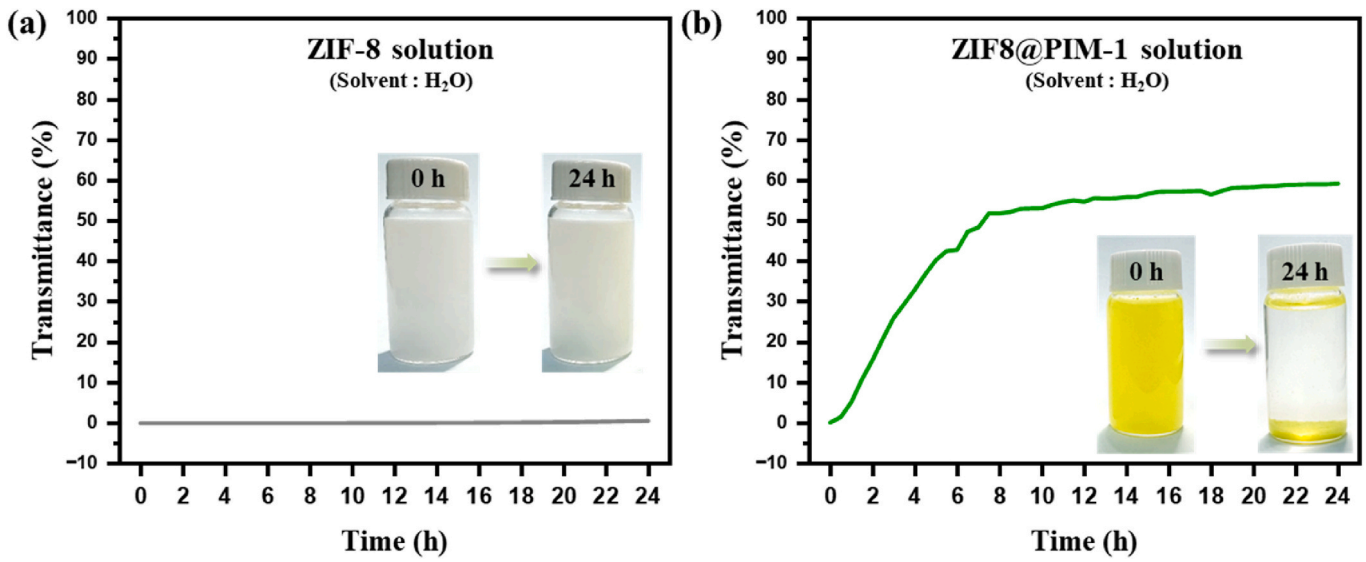

Fig. 3. Dispersion stability test of ZIF-8 and ZIF-8@PIM-1 solution in H_2O solvent (measurement point is 10 mm, total height is 40 mm).

Table 1
Bulk elemetal composition of ZIF-8, ZIF-8@PIM-1 particle, and PIM-1 powder obtained by elemental analysis.

Material	Zn (wt%)	C (wt%)	H (wt%)	N (wt%)	O (wt%)
ZIF-8	28.9	41.4	4.77	22.0	2.96
ZIF-8@PIM-1	26.8	44.5	4.80	20.4	3.58
PIM-1	–	74.1	4.24	5.98	14.0

a. The wt% of Zn is the total mass minus C, H, N, and O.

Table 2
BET surface area, pore volume and pore size of ZIF-8, ZIF-8@PIM-1 and PIM-1 powder.

Material	S_{BET} (m^2/g)	V_{total} (cm^3/g)	V_{micro} (cm^3/g)	Pore size (nm)
ZIF-8	1697	1.39	0.69	0.699
ZIF-8@PIM-1	1659	1.37	0.67	0.694
PIM-1	875	0.662	0.35	0.981

ZIF-@PIM-1 decreases at a constant ratio of 4.7–5.4 %, confirming the presence of a certain amount of PIM-1. X-ray diffraction (XRD) analysis was performed to confirm that the crystal structure of ZIF-8 was maintained even after the polymer was coated. Fig. 4c presents the XRD patterns of ZIF-8, ZIF-8@PIM-1, and PIM-1. ZIF-8 could confirm eight 2θ values at 7.3°, 10.35°, 12.7°, 14.8°, 16.4°, 18°, 24.5° and 26.7°, respectively, which correspond to ZIF-8. PIM-1 has an amorphous structure that does not exhibit crystallinity; therefore, its XRD pattern showed a broad peak. Because the ZIF-8@PIM-1 particle still showed the same 2θ structure as ZIF-8, the crystal structure was well maintained even after coating the polymer on the surface.

3.2. Characterization of MMMs

All the membranes were prepared using Pebax-1657 as the polymer matrix. Fig. S6 shows photographs of the prepared membrane. Pure Pebax-1657 exhibited a transparent color, whereas it was white and opaque when ZIF-8 was introduced as a filler. In addition, when ZIF-8@PIM-1 was introduced as the filler, it exhibited a yellow fluorescent color unique to PIM-1. SEM analysis and EDS mapping were performed to confirm the interfacial compatibility between the polymer matrix and the filler in a well-prepared membrane.

Fig. 5a–e and Fig. 5f–j shows the SEM surface and cross-sectional images of the MMMs, respectively. The pure Pebax-1657 membrane exhibited a smooth surface and cross-sectional image; however, when fillers were introduced, large amounts of ZIF-8 and ZIF-8@PIM-1 fillers were found. Another intrinsic problem with MMMs is that the fillers agglomerate or precipitate because of their low compatibility. To investigate this problem, EDS mapping of the cross-sectional SEM images was performed, as shown in Fig. 5o–r. Surface-modified ZIF-8 existed in a well-dispersed form within the MMMs. This suggests that the ZIF-8@PIM-1 filler was well-dispersed and existed within the polymer

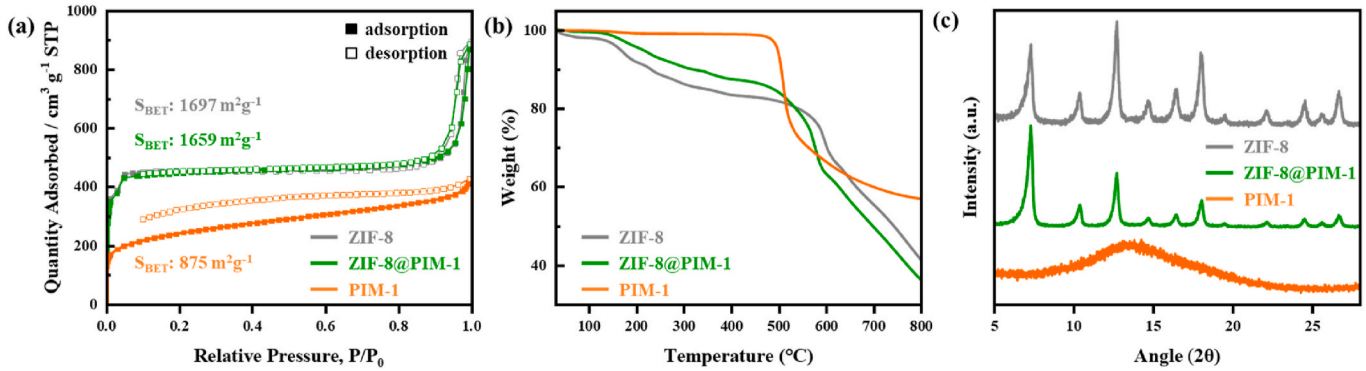

Fig. 4. (a) N_2 adsorption–desorption isotherms of ZIF-8, ZIF-8@PIM-1 particle, and PIM-1 powder at 77 K; (b) TGA result of ZIF-8, ZIF-8@PIM-1 particle, and PIM-1 powder; (c) XRD patterns of ZIF-8, ZIF-8@PIM-1 particle, and PIM-1 powder.

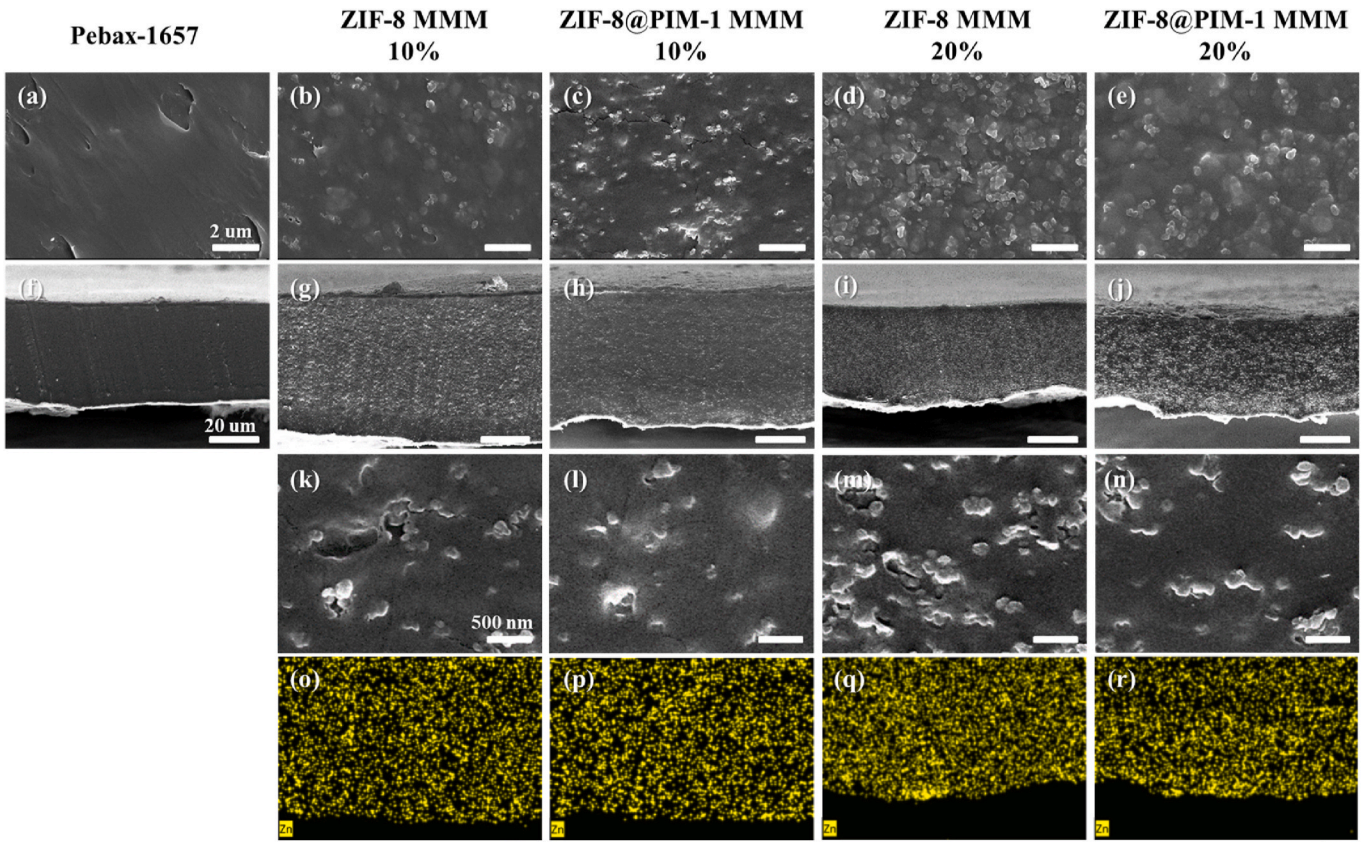

Fig. 5. SEM images of Pebax-1657 membrane, ZIF-8 MMMs, ZIF-8@PIM-1 MMMs. (a–e) surface SEM images; (f–n) cross-sectional SEM images; and (o–r) EDS mappings of the cross-sectional SEM images.

matrix. To examine in more detail the interfacial compatibility of the fillers with each polymer matrix, high-magnification cross-sectional SEM images were obtained, as shown in Fig. 5k–n. Fig. 5k and m shows cross-sectional SEM images of the ZIF-8 MMMs, while Fig. 5l and n shows cross-sectional images of the ZIF-8@PIM-1 MMMs. For the polymer-coated ZIF-8@PIM-1 MMMs, a defect-free pattern was observed with no nonselective pores around the fillers. For the ZIF-8 MMMs, multiple defects were observed, which reduced the selectivity when the gas passed through the membrane. Therefore, the interfacial compatibility between the filler and polymer matrix was enhanced through surface modification based on PIM-1.

Wide-angle X-ray scattering (WAXS) analysis was performed to confirm that the crystal structure of ZIF-8 was maintained on the membrane, as shown in Fig. 6. The WAXS peak of pure Pebax-1657 appears at 1.42 and 1.69 nm^{-1}, similar to that of pure Pebax-1657 with both rubbery PEO and glassy PA phases. The peak corresponding to the rigid PA phase showed stronger crystallinity owing to the inter-chain hydrogen bonds. The ZIF-8 MMMs exhibited the same q-value as the XRD pattern shown in Fig. 3b. Each peak appears at 0.52, 0.73, 0.90, 1.04, 1.16, 1.27, 1.72, and 1.87 nm^{-1}, and all of these peaks coincide with the eight peaks in the XRD data. The ZIF-8@PIM-1 MMMs showed the same tendency as the ZIF-8 MMMs, which proves that the crystal structure of ZIF-8 was well maintained in the MMMs.

3.3. Gas permeability and selectivity

Fig. 7 presents the gas permeability and selectivity of Pebax-1657 containing ZIF-8 and ZIF-8@PIM-1 MMMs as a function of the filler content. The permeability coefficients and selectivity values are listed in Table 3. The pure Pebax-1657 measured in this study exhibited a CO_2 permeability of 71 Barrer, with a CO_2/N_2 selectivity of 44.4 and a CO_2/CH_4 selectivity of 15.1, which are consistent with previously reported

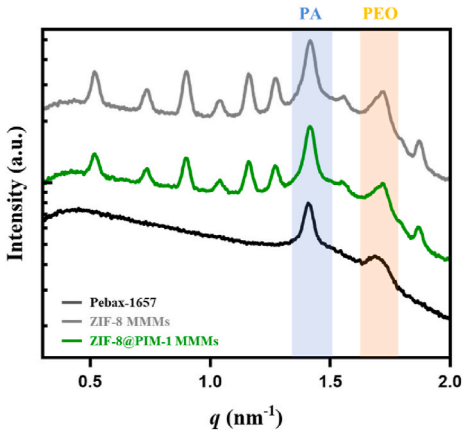

Fig. 6. Wide-angle x-ray scattering spectra of the Pebax-1657 membrane, ZIF-8 MMMs, and ZIF-8@PIM-1 MMMs.

values [47–49]. For Pebax-1657 containing ZIF-8 (Fig. 7a), the addition of ZIF-8 filler systematically increases CO_2 permeability. For example, at 20 wt% ZIF-8 loading, the CO_2 permeability increased by nearly 40 % compared to that of pure Pebax-1657. The CO_2/N_2 and CO_2/CH_4 selectivities remain similar with increasing ZIF-8 content up to 10 wt%. However, at loadings above 10 wt%, a noticeable decrease in CO_2/N_2 and CO_2/CH_4 selectivity was observed due to the formation of non-selective regions arising from interfacial voids, as confirmed by SEM analysis (cf. Section 3.2). These trends in permeability and selectivity are consistent with those observed for other polymeric membranes containing ZIF-8 fillers at high loadings [49–54].

To minimize the interfacial voids between the polymer and ZIF-8

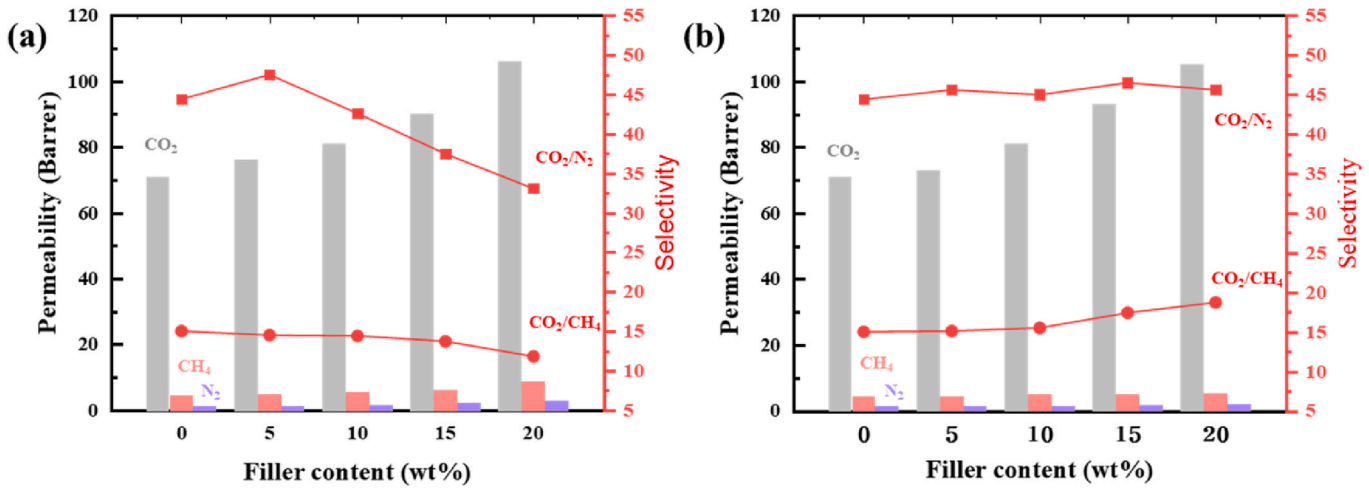

Fig. 7. Gas permeability and selectivity of (a) ZIF-8 MMMs and (b) ZIF-8@PIM-1 MMMs as a function of filler content (wt%) at 3 bar and 35 °C.

Table 3
Gas permeability and selectivity of Pebax-1657, ZIF-8, and ZIF-8@PIM-1 MMMs as a function of filler content (wt%) at 3 bar and 35 °C.

Membrane materials	Filler content (wt%)	Ideal permeability (barrer)			Ideal selectivity	
		P (CO_2)	P (N_2)	P (CH_4)	CO_2/N_2	CO_2/CH_4
Pebax-1657	0	71	1.6	4.7	44.4	15.1
ZIF-8 MMMs	5	76	1.6	5.2	47.5	14.6
	10	81	1.9	5.6	42.6	14.5
	15	90	2.4	6.5	37.5	13.8
	20	106	3.2	8.9	33.1	11.9
ZIF-8@PIM-1 MMMs	5	73	1.6	4.8	45.6	15.2
	10	81	1.8	5.2	45.0	15.6
	15	93	2.0	5.3	46.5	17.5
	20	105	2.3	5.6	45.6	18.8

filler, PIM-1 was coated onto the ZIF-8 surface. This coating strategy was designed to enhance the interfacial adhesion without obstructing the pore size and sorption capacity of ZIF-8 (Table 2). As shown in Fig. 7b, as the ZIF-8@PIM-1 filler content increased, the CO_2 permeability increased to an extent similar to that observed for Pebax-1657 containing ZIF-8. Interestingly, above 10 wt% loading, increasing the ZIF-8@PIM-1 content slightly enhances CO_2/CH_4 selectivity, which corresponded to the greatest difference in kinetic diameter in this study while maintaining a similar CO_2/N_2 selectivity. For example, at 20 wt% ZIF-8@PIM-1 loading, the CO_2/CH_4 selectivity increased by 20 % compared to that of pure Pebax-1657, from 15.1 to 18.7. These results suggest that coating ZIF-8 with PIM-1 can minimize interfacial voids (cf. Section 3.2), allowing the molecular sieving effect of ZIF-8 to contribute to more effective gas separation. The observed permeability trends are discussed in detail in terms of the contributions of diffusivity and solubility.

3.4. Gas solubility and diffusivity

Gas permeability in polymeric membranes is described by the solution-diffusion model, as shown in Eq. (4) [55]:

$$P = D \times S \quad (4)$$

where P is the gas permeability, D is the diffusion coefficient, and S is the solubility coefficient. In this study, the solubilities of Pebax-1657 and MMMs were measured using the pressure-decay method. Using the measured permeability and solubility coefficients, the diffusivity values were calculated based on Eq. (4).

Fig. 8 presents the diffusion coefficients and diffusivity selectivity of CO_2 and CH_4 for Pebax-1657 and MMMs. As shown in Fig. 8a, increasing the filler content of both ZIF-8 and ZIF-8@PIM-1 results in opposite trends for CO_2 and CH_4 diffusivity in the MMMs. For both MMMs, CO_2 diffusivity increases slightly as the filler content increases, while the CH_4 diffusivity decreases. This trend is attributed to the molecular sieving effect of ZIF-8, which has an effective pore aperture size of approximately 0.40 nm [48,49]. The presence of ZIF-8 in the MMMs can facilitate the transport of smaller CO_2 molecules (kinetic diameter: 0.33 nm). In contrast, the diffusion of larger CH_4 molecules (kinetic diameter: 0.38 nm) can be hindered, forcing them to follow tortuous pathways within the MMMs, leading to a decrease in CH_4 diffusivity [54,56].

For both MMMs in this study, CO_2 diffusivity increases slightly as the filler content increases. At 20 wt% filler loading, CO_2 diffusivity in both MMMs increases by about 30 %. However, the trends for CH_4 diffusivity differ between the two MMMs. For the MMMs containing ZIF-8, CH_4 diffusivity decreases up to 15 wt% filler loading and then increases noticeably at 20 wt%, In contrast, for the MMMs containing ZIF-8@PIM-1, CH_4 diffusivity decreases progressively and to a greater extent as the filler content increases. As shown in Fig. 8b, CO_2/CH_4 diffusivity selectivity increases with ZIF-8 content, but to a lesser extent than in the MMMs containing ZIF-8@PIM-1. The diffusivity selectivity reached a maximum at 15 wt% ZIF-8 loading and then decreased, suggesting the formation of interfacial voids at higher filler contents. In contrast, for the MMMs containing ZIF-8@PIM-1, CO_2/CH_4 diffusivity selectivity increases consistently with increasing filler content. This trend supports the enhanced interfacial adhesion between ZIF-8@PIM-1 and Pebax-1657, highlighting that the molecular sieving effect was facilitated by the minimized interfacial voids. Additionally, as discussed earlier (Section 3.1), the pore sizes of ZIF-8 and ZIF-8@PIM-1 are very similar. This suggests that the observed increases in diffusivity selectivity are primarily due to improved interfacial adhesion, rather than differences in pore size.

Fig. 9 presents the solubility coefficients and solubility selectivities of CO_2 and CH_4 for Pebax-1657 and MMMs at 3 bar and 35 °C. The sorption isotherms are shown in Fig. S8. As shown in Fig. 9a, the addition of both ZIF-8 and ZIF-8@PIM-1 fillers, along with increasing filler content, results in similar changes in CO_2 and CH_4 solubility, leading to comparable increases in solubility in both MMMs. For both MMMs, the CH_4 solubility increased significantly more than the CO_2 solubility as the filler content increased. Consequently, as shown in Fig. 9b, the CO_2/CH_4 solubility selectivity decreases with increasing filler content. Overall, based on the results in Figs. 8 and 9 for the MMMs containing ZIF-8@PIM-1, the observed increases in CO_2 permeability with filler content are due to increases in both solubility and diffusivity, whereas the

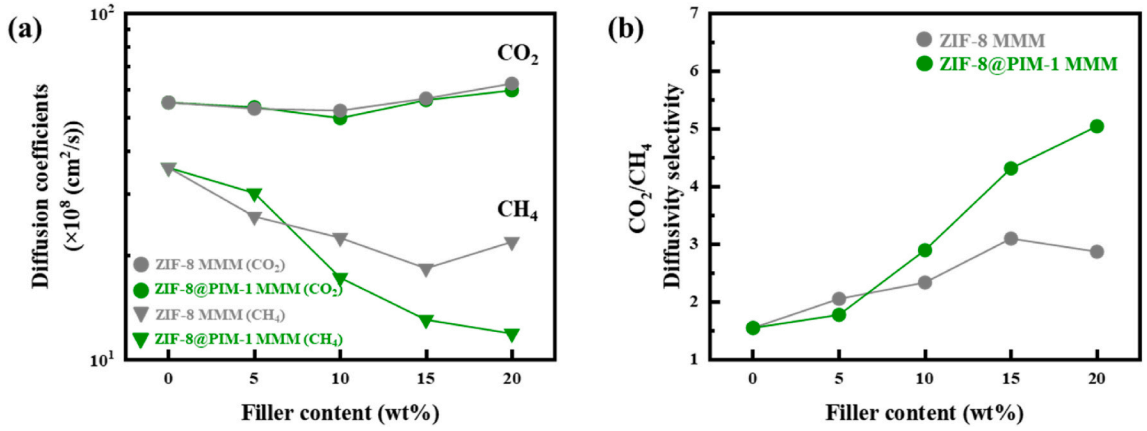

Fig. 8. (a) Diffusion coefficients and (b) diffusivity selectivity of CO_2 and CH_4 for the MMMs as a function of filler content (wt%) at 3 bar and 35 °C.

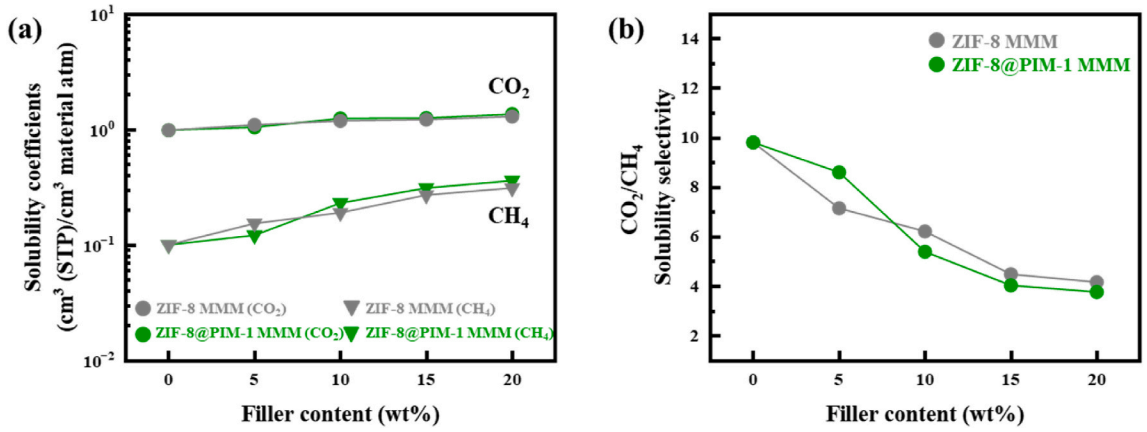

Fig. 9. (a) Solubility coefficients and (b) solubility selectivity of CO_2 and CH_4 for the MMMs as a function of filler content (wt%) at 3 bar and 35 °C.

enhancement in CO_2/CH_4 permeability selectivity is due to a significant increase in diffusivity selectivity. The data shown in Figs. 8 and 9 are summrized in Table S1.

To further support the observed solubility and solubility selectivity results, the CO_2 and CH_4 solubilities of pure ZIF-8 and pure ZIF-8@PIM-1 fillers were measured and compared with those of pure Pebax-1657 (Fig. S7). The gas solubilities of the ZIF-8 and ZIF-8@PIM-1 fillers are nearly identical, further confirming that PIM-1 has little impact on the sorption capacity of ZIF-8. In addition, both fillers exhibited significantly higher gas solubilities than pure Pebax-1657. For example, CO_2 and CH_4 solubility coefficients in ZIF-8 and ZIF-8@PIM-1 fillers are 4 and 18 times higher, respectively, than those in pure Pebax-1657. This suggests that the results in Fig. 9 are reasonable, as the addition of these fillers – both of which have higher sorption capacity but lower solubility selectivity than pure Pebax-1657 – enhances gas solubility while simultaneously decreasing solubility selectivity in the MMMs.

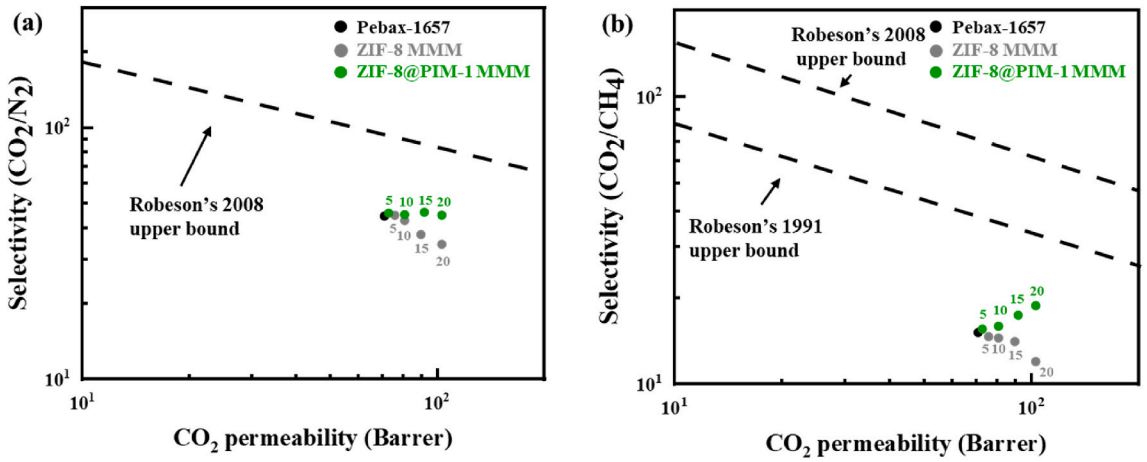

Fig. 10. (a) CO_2/N_2 and (b) CO_2/CH_4 separation performances of Pebax-1657, ZIF-8, and ZIF-8@PIM-1 MMMs with various filler loadings (5, 10, 15, 20 wt%) at 3 bar and 35 °C in the upper bound plots.

Fig. 10 presents the Robeson upper bound plots for the CO_2/N_2 and CO_2/CH_4 gas pairs in the MMMs. For the MMMs containing ZIF-8, the CO_2 permeability increases at the expense of both CO_2/N_2 selectivity (Fig. 10a) and CO_2/CH_4 selectivity (Fig. 10b) as the filler content increases, indicating a significant trade-off between permeability and selectivity. This trade-off becomes more pronounced at higher filler loadings owing to the formation of interfacial voids. However, in the MMMs containing ZIF-8@PIM-1, the enhanced interfacial adhesion provided by the PIM-1 coating mitigated the formation of interfacial voids, thereby counterbalancing the reduction in selectivity. Notably, for the CO_2/CH_4 pair, which exhibits the greatest difference in kinetic diameter in this study, increasing ZIF-8@PIM-1 content shifts the transport properties toward the upper-right of the Robeson plot. This suggests that coating ZIF-8 with PIM-1 enhances the molecular sieving effect of ZIF-8, leading to more effective gas separation.

4. Conclusions

We addressed the interfacial issues arising from the incorporation of high-loading ZIF-8 into Pebax-1657-based mixed-matrix membranes (MMMs) through PIM-1-based surface modification. Surface modification was performed using NISD, and the successful fabrication of ZIF-8@PIM-1 was confirmed through TEM, SEM, UV–Vis DRS spectroscopy, dispersion stability tests, FT-IR, EA, and XPS. Furthermore, the physical properties of ZIF-8@PIM-1 were characterized using N_2 adsorption, TGA, and XRD, demonstrating that the unique crystalline structure and high BET surface area were maintained post-modification, effectively preventing pore blockage. SEM and WAXS analyses of the MMMs incorporating ZIF-8 and ZIF-8@PIM-1 as fillers showed that Pebax-1657-based MMMs containing ZIF-8@PIM-1 maintained their structural integrity without forming significant interfacial voids, even at a high loading of 20 wt%, indicating that PIM-1-based surface modification effectively resolved interfacial issues. The gas transport results further demonstrated that the surface modification enhanced the performance of the MMMs at high loading. This enhancement was primarily attributed to the improved interfacial adhesion, which minimized non-selective voids, thereby effectively promoting the molecular sieving of ZIF-8. Additionally, the gas sorption results supported that the enhanced selectivity was primarily diffusion-related. This new strategy is expected to be applicable to a variety of polymer matrices offering an effective solution for addressing the interfacial challenges of MMMs. Future studies are expected to enable the fabrication of MMMs with even higher loadings and excellent selectivities by employing PIM-1 with functional groups capable of forming diverse chemical bonds with the polymer matrices.

CRediT authorship contribution statement

Chanhyuk Kang: Writing – original draft, Investigation, Conceptualization. **Yeji Moon:** Writing – original draft, Investigation, Conceptualization. **Joo Eon Kim:** Investigation, Data curation. **Hyojin Kim:** Investigation, Data curation. **Jinhan Cho:** Conceptualization. **Jinkee Hong:** Writing – review & editing, Conceptualization. **Jaesung Park:** Writing – review & editing, Conceptualization. **Byoung Gak Kim:** Writing – review & editing, Funding acquisition, Conceptualization.

Declaration of competing interest

The authors declare that they have no known competing financial interests or personal relationships that could have appeared to influence the work reported in this paper.

Acknowledgements

This study was supported by the Korea Research Institute of Chemical Technology (KRICT) Core Program (grant number KS2422-20). This study was partially supported by a government-sponsored project (KN24-112) of the Ministry of Science and ICT (MSIT). This research was supported by a government-sponsored project (IJ23-06R) of the Ministry of SMEs and Startups (MSS).

Appendix A. Supplementary data

Supplementary data to this article can be found online at https://doi.org/10.1016/j.memsci.2025.123838.

Data availability

Data will be made available on request.

References

[1] D. Aaron, C. Tsouris, Separation of CO2 from flue gas: a review, Separ. Sci. Technol. 40 (1–3) (2005) 321–348.
[2] A. Brunetti, et al., Membrane technologies for CO2 separation, J. Membr. Sci. 359 (1–2) (2010) 115–125.
[3] L.M. Robeson, Polymer membranes for gas separation, Curr. Opin. Solid State Mater. Sci. 4 (6) (1999) 549–552.
[4] Y. Yampolskii, Polymeric gas separation membranes, Macromolecules 45 (8) (2012) 3298–3311.
[5] K. Ghosal, B.D. Freeman, Gas separation using polymer membranes: an overview, Polym. Adv. Technol. 5 (11) (1994) 673–697.
[6] J.D. Wind, et al., The effects of crosslinking chemistry on CO2 plasticization of polyimide gas separation membranes, Ind. Eng. Chem. Res. 41 (24) (2002) 6139–6148.
[7] Y. Liu, R. Wang, T.-S. Chung, Chemical cross-linking modification of polyimide membranes for gas separation, J. Membr. Sci. 189 (2) (2001) 231–239.
[8] G. Chowdhury, B. Kruczek, T. Matsuura, Polyphenylene Oxide and Modified Polyphenylene Oxide Membranes: Gas, Vapor, and Liquid Separation, Springer Science & Business Media, 2001.
[9] F. Hamad, K. Khulbe, T. Matsuura, Characterization of gas separation membranes prepared from brominated poly (phenylene oxide) by infrared spectroscopy, Desalination 148 (1–3) (2002) 369–375.
[10] V. Vatanpour, et al., Cellulose acetate in fabrication of polymeric membranes: a review, Chemosphere 295 (2022) 133914.
[11] G.Q. Chen, et al., Water vapor permeation through cellulose acetate membranes and its impact upon membrane separation performance for natural gas purification, J. Membr. Sci. 487 (2015) 249–255.
[12] M. Hussain, A. Koenig, Mixed-matrix membrane for gas separation: polydimethylsiloxane filled with zeolite, Chem. Eng. Technol. 35 (3) (2012) 561–569.
[13] H.B. Park, et al., Maximizing the right stuff: the trade-off between membrane permeability and selectivity, Science 356 (6343) (2017) eaab0530.
[14] B.D. Freeman, Basis of permeability/selectivity tradeoff relations in polymeric gas separation membranes, Macromolecules 32 (2) (1999) 375–380.
[15] N. Du, et al., Advances in high permeability polymeric membrane materials for CO 2 separations, Energy Environ. Sci. 5 (6) (2012) 7306–7322.
[16] M. Aroon, et al., Performance studies of mixed matrix membranes for gas separation: a review, Sep. Purif. Technol. 75 (3) (2010) 229–242.
[17] P. Goh, et al., Recent advances of inorganic fillers in mixed matrix membrane for gas separation, Sep. Purif. Technol. 81 (3) (2011) 243–264.
[18] G. Dong, H. Li, V. Chen, Challenges and opportunities for mixed-matrix membranes for gas separation, J. Mater. Chem. A 1 (15) (2013) 4610–4630.
[19] B. Seoane, et al., Metal–organic framework based mixed matrix membranes: a solution for highly efficient CO 2 capture? Chem. Soc. Rev. 44 (8) (2015) 2421–2454.
[20] M. Al-Shaeli, et al., Long-term stable metal organic framework (MOF) based mixed matrix membranes for ultrafiltration, J. Membr. Sci. 635 (2021) 119339.
[21] M.J.C. Ordonez, et al., Molecular sieving realized with ZIF-8/Matrimid® mixed-matrix membranes, J. Membr. Sci. 361 (1–2) (2010) 28–37.
[22] M. Benzaqui, et al., Toward an understanding of the microstructure and interfacial properties of PIMs/ZIF-8 mixed matrix membranes, ACS Appl. Mater. Interfaces 8 (40) (2016) 27311–27321.
[23] R. Nasir, et al., Material advancements in fabrication of mixed-matrix membranes, Chem. Eng. Technol. 36 (5) (2013) 717–727.
[24] H. Ren, et al., Affinity between metal–organic frameworks and polyimides in asymmetric mixed matrix membranes for gas separations, Ind. Eng. Chem. Res. 51 (30) (2012) 10156–10164.
[25] H. Zhu, et al., Improved interfacial affinity and CO2 separation performance of asymmetric mixed matrix membranes by incorporating postmodified MIL-53 (Al), ACS Appl. Mater. Interfaces 8 (34) (2016) 22696–22704.
[26] S. Yu, et al., Recent advances in the interfacial engineering of MOF-based mixed matrix membranes for gas separation, Nanoscale 16 (2024) 7716–7733.
[27] R. Thür, et al., Correlating MOF-808 parameters with mixed-matrix membrane (MMM) CO 2 permeation for a more rational MMM development, J. Mater. Chem. A 9 (21) (2021) 12782–12796.

[28] B. Ghalei, et al., Enhanced selectivity in mixed matrix membranes for CO2 capture through efficient dispersion of amine-functionalized MOF nanoparticles, Nat. Energy 2 (7) (2017) 1–9.
[29] L. Gong, et al., Ionic liquid enhancement of interface compatibility in mixed-linker ZIF-based mixed matrix membranes for advanced CO 2/CH 4 separation, J. Mater. Chem. A 10 (47) (2022) 24975–24984.
[30] N. Habib, et al., A novel IL/MOF/polymer mixed matrix membrane having superior CO2/N2 selectivity, J. Membr. Sci. 658 (2022) 120712.
[31] C. Wu, et al., Enhancing the gas separation selectivity of mixed-matrix membranes using a dual-interfacial engineering approach, J. Am. Chem. Soc. 142 (43) (2020) 18503–18512.
[32] Z. Wang, et al., Interfacial design of mixed matrix membranes for improved gas separation performance, Adv. Mater. 28 (17) (2016) 3399–3405.
[33] K. Xie, et al., Increasing both selectivity and permeability of mixed-matrix membranes: sealing the external surface of porous MOF nanoparticles, J. Membr. Sci. 535 (2017) 350–356.
[34] Y. Katayama, K.C. Bentz, S.M. Cohen, Defect-free MOF-based mixed-matrix membranes obtained by corona cross-linking, ACS Appl. Mater. Interfaces 11 (13) (2019) 13029–13037.
[35] C. Wu, et al., One-step rapid fabrication of MOF@ polymer core–shell particles through non-solvent induced surface deposition, J. Mater. Chem. A 10 (46) (2022) 24676–24684.
[36] P.M. Budd, et al., Gas permeation parameters and other physicochemical properties of a polymer of intrinsic microporosity: polybenzodioxane PIM-1, J. Membr. Sci. 325 (2) (2008) 851–860.
[37] J.W. Jeon, et al., Highly carboxylate-functionalized polymers of intrinsic microporosity for CO2-selective polymer membranes, Macromolecules 50 (20) (2017) 8019–8027.
[38] Y. Zhang, et al., Pebax mixed-matrix membrane with highly dispersed ZIF-8@ CNTs to enhance CO2/N2 separation, ACS Omega 6 (29) (2021) 18566–18575.
[39] Z.P. Smith, et al., Gas sorption and characterization of thermally rearranged polyimides based on 3, 3′-dihydroxy-4, 4′-diamino-biphenyl (HAB) and 2, 2′-bis-(3, 4-dicarboxyphenyl) hexafluoropropane dianhydride (6FDA), J. Membr. Sci. 415 (2012) 558–567.
[40] H. Lin, B. Freeman, Permeation and Diffusion, Springer, New York, 2006, pp. 371–387.
[41] E. Burnett, Compressibility determinations without volume measurements, J. Appl. Mech. 3 (1936) 136–140.
[42] S. Matteucci, et al., Transport of gases and vapors in glassy and rubbery polymers, Mater. Sci. Membr. Gas Vapor Separ. 1 (2006) 1–2.
[43] C. Zhang, et al., High performance ZIF-8/6FDA-DAM mixed matrix membrane for propylene/propane separations, J. Membr. Sci. 389 (2012) 34–42.
[44] N.A.H.M. Nordin, et al., Facile modification of ZIF-8 mixed matrix membrane for CO 2/CH 4 separation: synthesis and preparation, RSC Adv. 5 (54) (2015) 43110–43120.
[45] Y.C. Chiang, W.T. Chin, Preparation of zeolitic imidazolate framework-8-based nanofiber composites for carbon dioxide adsorption, Nanomaterials (Basel) 12 (9) (2022).
[46] A. Awadallah-F, et al., On the nanogate-opening pressures of copper-doped zeolitic imidazolate framework ZIF-8 for the adsorption of propane, propylene, isobutane, and n-butane, J. Mater. Sci. 54 (7) (2018) 5513–5527.
[47] D. Nobakht, R. Abedini, Improved gas separation performance of Pebax® 1657 membrane modified by poly-alcoholic compounds, J. Environ. Chem. Eng. 10 (3) (2022) 107568.
[48] M. Li, et al., Pebax-based composite membranes with high gas transport properties enhanced by ionic liquids for CO 2 separation, RSC Adv. 7 (11) (2017) 6422–6431.
[49] S. Meshkat, S. Kaliaguine, D. Rodrigue, Comparison between ZIF-67 and ZIF-8 in Pebax® MH-1657 mixed matrix membranes for CO2 separation, Sep. Purif. Technol. 235 (2020) 116150.
[50] X. Zhang, et al., Mixed-matrix membranes based on Zn/Ni-ZIF-8-PEBA for high performance CO2 separation, J. Membr. Sci. 560 (2018) 38–46.
[51] H. Li, et al., Simultaneous enhancement of mechanical properties and CO2 selectivity of ZIF-8 mixed matrix membranes: interfacial toughening effect of ionic liquid, J. Membr. Sci. 511 (2016) 130–142.
[52] X. Wang, et al., Sealing Tröger base/ZIF-8 mixed matrix membranes defects for improved gas separation performance, J. Membr. Sci. 636 (2021) 119582.
[53] Y. Fan, et al., Zn (II)-modified imidazole containing polyimide/ZIF-8 mixed matrix membranes for gas separations, J. Membr. Sci. 597 (2020) 117775.
[54] K. Chen, et al., Phenolic resin regulated interface of ZIF-8 based mixed matrix membrane for enhanced gas separation, J. Membr. Sci. 666 (2023) 121117.
[55] J.G. Wijmans, R.W. Baker, The solution-diffusion model: a review, J. Membr. Sci. 107 (1–2) (1995) 1–21.
[56] Y. Liu, et al., Upgrading CO2/CH4 separation performances of Pebax-based mixed-matrix membranes incorporated with core/shell-structured ZIF-L (Co)@ ZIF-8 composite nanosheets, J. Membr. Sci. 659 (2022) 120787.